Civil Engineering Dimension
https://ced.petra.ac.id

Finite Element Analysis of Plastic Behavior in RC Beam Supports with Composite Steel Deck Slabs under Cyclic Loading

Brihaspati[1], Saputra, A.[1]*, Setiawan, A.F.[1], and Sulistyo, D.[1]
[1] Department of Civil and Environmental Engineering, Universitas Gadjah Mada
Jl. Grafika Kampus No. 2, Senolowo, Sinduadi, Mlati, Sleman, Yogyakarta 55284, INDONESIA

DOI: https://doi.org/10.9744/ced.28.1.34-45

Article Info:
Submitted: May 26, 2025
Reviewed: June 28, 2025
Accepted: Dec 09, 2025

Keywords:
beam-column,
steel deck,
plastic behavior,
hysteresis loop,
ABAQUS.

Corresponding Author:
Saputra, A.
Department of Civil and Environmental Engineering, Universitas Gadjah Mada
Jl. Grafika Kampus No. 2, Senolowo, Sinduadi, Mlati, Sleman,
Yogyakarta 55284, INDONESIA
Email: saputra@ugm.ac.id

Abstract

The performance of beam supports is essential for seismic resilience, particularly under the Strong Column–Weak Beam (SCWB) principle. To improve construction efficiency, steel deck-based composite slabs are increasingly adopted as alternatives to conventional slabs. However, their impact on the plastic behavior of beam supports remains underexplored. This study evaluates the influence of steel deck slabs using finite element analysis in ABAQUS. Two beam-column joint models—conventional and modified—were subjected to cyclic loading according to FEMA 461. The models incorporated stiffness recovery, combined hardening for steel, and a cohesive zone model (CZM) for the concrete–steel deck interface. Results indicate that the steel deck model shows a wider hysteresis loop and 2.425% higher energy dissipation, but experiences earlier reinforcement yielding and greater stiffness degradation. Although ductility increases, plastic hinges form at nearly the same cycle. Overall, the steel deck system improves energy absorption and ductility but reduces elastic stiffness and accelerates inelastic behavior.

INTRODUCTION

The performance of building structures, particularly beam elements at supports, is critical for stability and safety, especially in earthquake-resistant design based on the Strong Column-Weak Beam (SCWB) principle. This principle ensures beam failure before column failure, enabling effective energy dissipation. In modern construction, steel deck composite slabs are widely used for their time and cost efficiency. However, their impact on structural behavior, particularly at beam supports, requires further investigation to ensure overall performance and safety.

Reinforced concrete beam-column joints under cyclic loading have been extensively studied to assess key factors affecting their performance. Experimental investigations show that concrete compressive strength is a dominant factor in joint shear capacity, while increased stirrup quantity significantly controls deformation in later stages [1]. Three-dimensional numerical analyses confirm these findings, revealing that column axial load and beam longitudinal reinforcement ratio have a minor effect, whereas joint aspect ratio enhances initial shear strength and delays cracking, despite shear degradation post-reinforcement yielding [2]. Other studies show that doubling shear reinforcement ratio has limited impact on load capacity, while reducing it weakens the joint; better hysteretic response and plastic hinge formation are observed with diagonal and transverse reinforcement [3]. The effect of floor slabs has also been explored, with slabs increasing negative flexural strength, stiffness, and energy dissipation, though

Note : Discussion is expected before July, 1st 2026, and will be published in the "Civil Engineering Dimension", volume 28, number 2, September 2026.
ISSN : 1410-9530 print / 1979-570X online
Published by : **Petra Christian University**

stiffness degrades in the positive direction under repeated cycles [4]. Joints with low-quality materials and inadequate reinforcement detailing show that anchorage length and anchoring systems are critical for energy dissipation and joint integrity, with bar slip and pullout being major failure causes [5]. Studies on composite slabs with steel decks suggest they offer comparable flexural capacity to conventional T-beams while reducing structural weight [6], though they lead to increased deflection that must be considered in design [7].

While research on beam-column joints under cyclic loading is extensive, studies on the impact of steel deck integration in reinforced concrete beams are limited. Further investigation is needed to assess the contribution of steel decks to the structural behavior of beams, particularly regarding plastic behavior at beam supports. This study aims to examine the impact of steel deck composite slabs on the flexural behavior of beam-column joints under cyclic loading, focusing on hysteresis loop shape, energy dissipation, ductility, stiffness, plastic hinge formation, and overall plastic performance through finite element analysis.

METHODS

Modeling and Validation against Previous Experimental Research

The numerical model was validated in two stages. First, against Durrani and Zerbe's experimental data [4] to ensure accurate cyclic response and failure patterns. Second, against Hedaoo et al.'s data [8] to validate the steel deck-concrete interaction, focusing on bond-slip behavior. The first validation replicated Durrani and Zerbe's experimental setup [4] in ABAQUS, modeling concrete with 8-node hexahedral elements (C3D8R) and reinforcement with 3D truss elements (T3D2), as shown in Figure 1. Elastic concrete was assigned to beam and column ends to prevent localized damage from boundary effects. A fixed length of 100 mm, equivalent to approximately 5% of the total column length, was used for the elastic zone. This was found to be sufficient to reduce artificial stress concentrations near the boundaries without affecting the global structural response. Analysis used the ABAQUS/Explicit solver with double precision to enhance accuracy, necessary due to the high element count (18,643), small time and length scales, and complex material interactions.

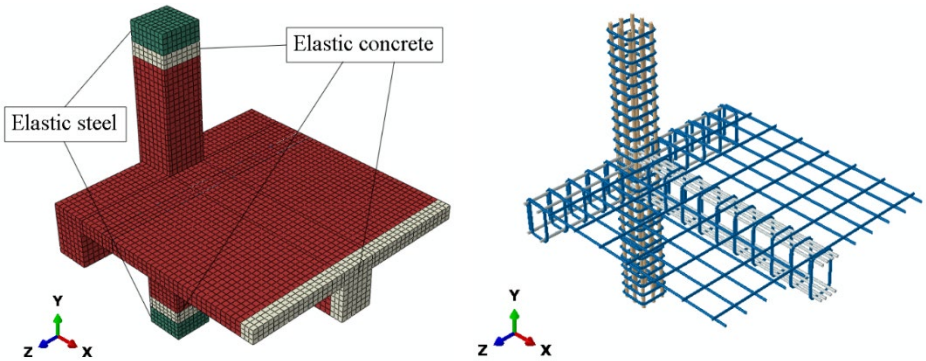

Figure 1. Finite Element Model of First Validation

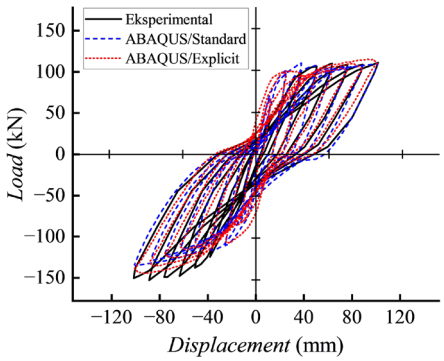

Figure 2. Hysteresis Loop Result of First Validation

The compressive stress-strain behavior of concrete was defined using the unconfined model by Mander et al. [9], while a bilinear model was applied for tensile behavior, acknowledging concrete's tensile strength as approximately 10% of its compressive strength. The Concrete Damaged Plasticity (CDP) model was employed to simulate inelastic

concrete behavior, with parameters provided in Table 1. Reinforcing steel was modeled using combined hardening plasticity, based on Narendra et al. [10] with adjustments. A discrete crack model was used to simulate macro crack propagation, accurately representing cracking once tensile stress surpassed the concrete's tensile capacity.

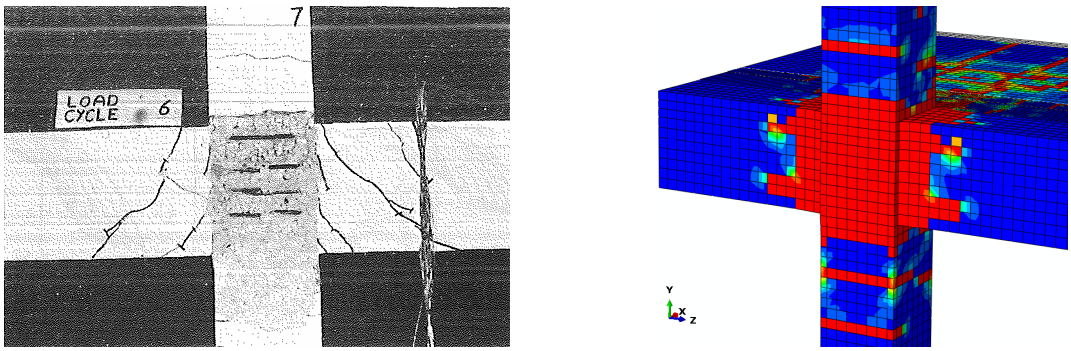

(a) Experimental [4] (b) Simulation Result

Figure 3. Damage Pattern Result of First Validation

The first validation results in Figure 2 and Figure 3 show strong agreement between the numerical and experimental data by Durrani and Zerbe [4]. The hysteresis loop captures key behaviors, such as pinching, stiffness degradation, and loop widening, despite minor discrepancies from modeling assumptions. Damage patterns, including shear cracks, concrete spalling, and torsion-induced failures, align well with experimental observations, confirming the model's accuracy for analyzing steel deck composite slab applications.

The second validation employed experimental data from Hedaoo et al. [8] to assess the response of the steel deck and its interaction with concrete. Similar element types were used as in the first validation, with the addition of S4R shell elements for the steel deck and rigid body elements for load transfer, as shown in Figure 4. The analysis was conducted in ABAQUS/Explicit using double precision and a total of 24,024 elements. Concrete was modeled following the first validation approach, while the steel deck was represented as structural steel using the Park and Paulay constitutive model [11] due to limited material data.

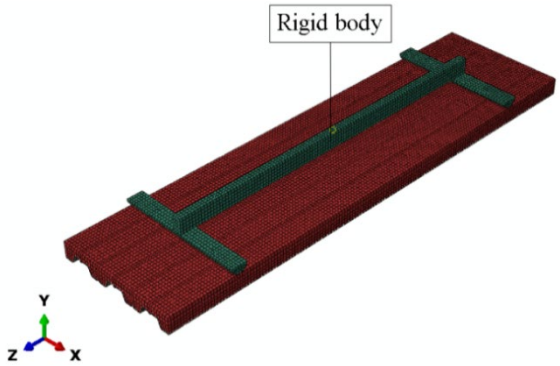

Figure 4. Finite Element Model of Second Validation

The concrete–steel deck interface was modeled using a Cohesive Zone Model (CZM) with a triangular damage law to capture failure from friction and adhesion loss. A traction–separation law with 100 N/mm³ stiffness was applied, assuming equal normal and shear stiffness (Knn = Kss = Ktt). Damage initiation followed a maximum nominal stress criterion, and its evolution was energy-based, with parameters from Hedaoo et al. [8] and Majdi et al. [12]. Normal and tangential contact with a friction coefficient of 0.3 defined the interaction between the rigid body and concrete. As the rigid body was assumed to be steel and served as a load spreader, a coefficient of 0.3 was adopted to represent typical dry friction between steel and concrete [13]. Degrees of freedom in rigid body were all restrained except in the loading direction to prevent rigid body motion and ensure numerical stability. Monotonic loading was applied incrementally at 0.25-second intervals to minimize dynamic effects and energy spikes. The second validation focused on concrete–steel deck interaction, comparing load–displacement curves from numerical simulation and experimental results by Hedaoo et al. [8], as shown in Figure 5. Additionally, damage patterns from the simulation were compared with experimental observations as shown in Figure 6. This validation aimed to refine the numerical modeling approach for beam–column joints and accurately represent the concrete–steel deck interaction in composite slabs.

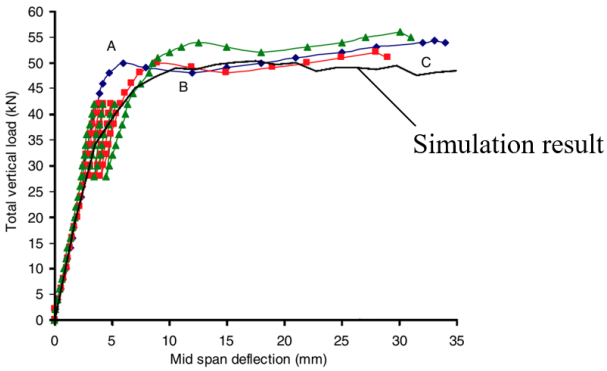

Figure 5. Load-displacement Result of Second Validation

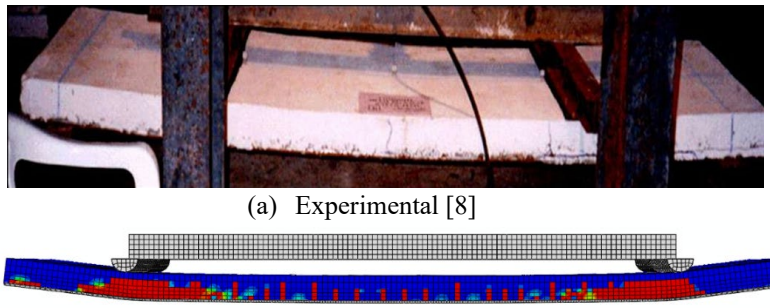

(a) Experimental [8]

(b) Simulation Result

Figure 6. Damage Pattern Result of Second Validation

Parametric Study

The two-stage validation results serve as the foundation for the subsequent numerical modeling. A parametric study was then conducted to assess the impact of steel deck application, using the geometry and material properties of an existing beam-column joint as the baseline configuration. Figure 7 illustrates the geometry and reinforcement configuration of the reinforced concrete beam-column joint, wherein the modified model, slab reinforcement is partially replaced by a profiled steel deck. The steel deck used in the composite slab model refers to the profile and material properties reported by Hedaoo et al. [8]. This includes the deck geometry, thickness, and mechanical behavior, particularly its bond-slip interaction with concrete. Both models maintain consistent overall dimensions and longitudinal reinforcement layouts in the beams and columns, with differences concentrated in the slab detailing.

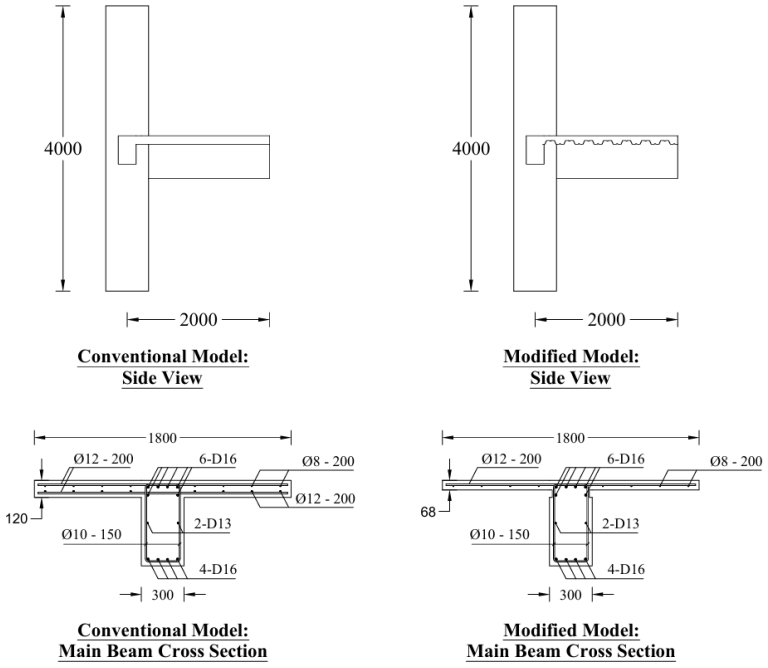

Figure 7. Geometry and Reinforcement Configuration of RC Beam-Column Joint

Numerical simulations were performed using ABAQUS/Explicit due to its capability to capture complex nonlinear material behavior and contact interactions under cyclic loading. Two three-dimensional finite element configurations were developed: (1) a conventional reinforced concrete beam-column joint and (2) a composite slab system incorporating a steel deck as a substitute for bottom slab reinforcement, as shown in Figure 8 and Figure 9. Boundary conditions were applied at the top and bottom column ends by restraining displacements (U1 = U2 = U3 = 0) along a central transverse line on each end surface.

Cyclic loading was imposed at the free end of the main beam using a displacement-controlled protocol. The loading was applied through a reference point located 100 mm away from the beam cross-section and connected to the beam surface using a kinematic coupling constraint, ensuring uniform displacement transfer.

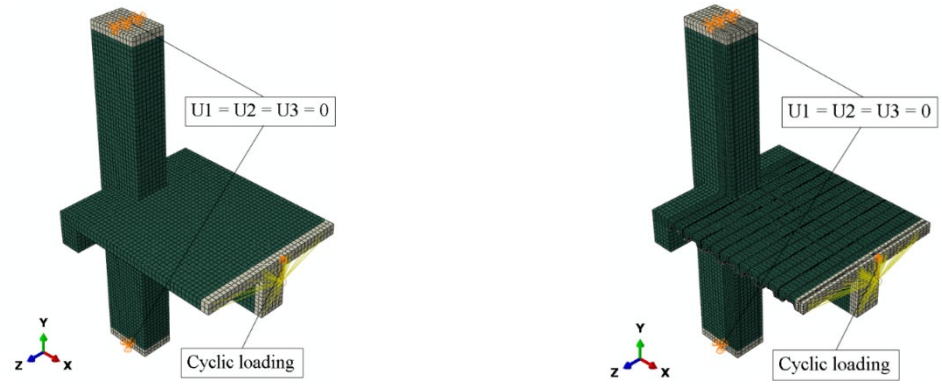

(a) Conventional Model (b) Modified Model

Figure 8. Finite Element Model of RC Beam-Column Joint

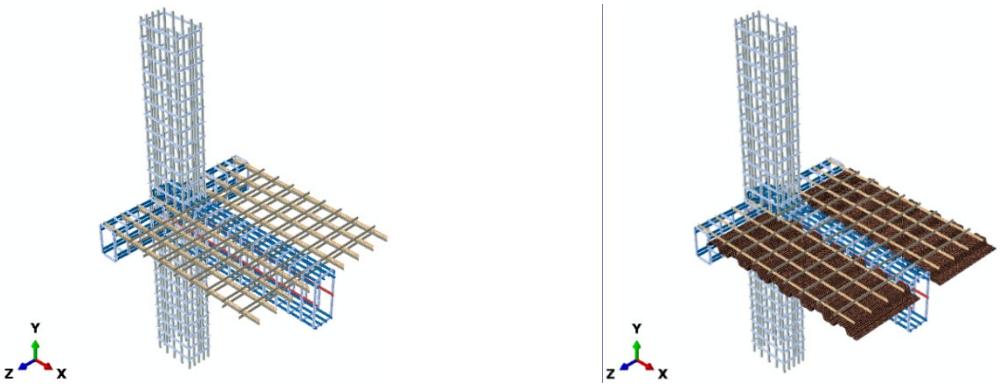

(a) Conventional Model (b) Modified Model

Figure 9. Finite Element Model of Reinforcement Layout in the RC Beam-Column Joint

Concrete Modeling

The compressive and tensile behavior of concrete (f'_c = 24.9 MPa) was modeled using the constitutive approach established during the first validation stage. These material responses are illustrated in Figure 10. The tensile strength was estimated as approximately 10 percent of the compressive strength, following the ACI 318M-14 equation.

$$f_t = 0.62\sqrt{f'_c} \tag{1}$$

The corresponding tensile strain at peak stress was calculated by dividing the tensile strength by the modulus of elasticity, assuming linear elastic behavior up to cracking.

Table 1. Concrete Damaged Plasticity (CDP) Parameters

ψ	ϵ	K_c	σ_{b0}/σ_{c0}	Viscosity
38°	0.1	0.6667	1.16	0.0005

The plastic behavior of concrete is represented using the Concrete Damaged Plasticity (CDP) model. In the CDP model, several parameters must be defined to capture the plastic response of the concrete material, including the dilation angle (ψ), eccentricity (ϵ), the shape factor of the yield surface (K_c), the ratio of biaxial to uniaxial

compressive strength (σ_{b0}/σ_{c0}), and the viscosity parameter. These parameters were determined through an initial validation process and are presented in Table 1.

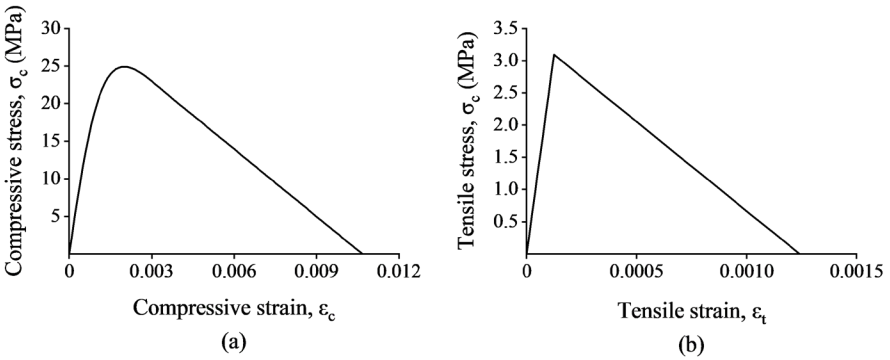

Figure 10. Concrete Material Model: (a) Compressive Behavior, and (b) Tensile Behavior

Since the applied load is cyclic, the concrete experiences a stiffness recovery effect during each loading cycle. As shown in Figure 11, during the transition phase from compression to tension, the damaged concrete does not exhibit tension stiffness recovery [14,15].

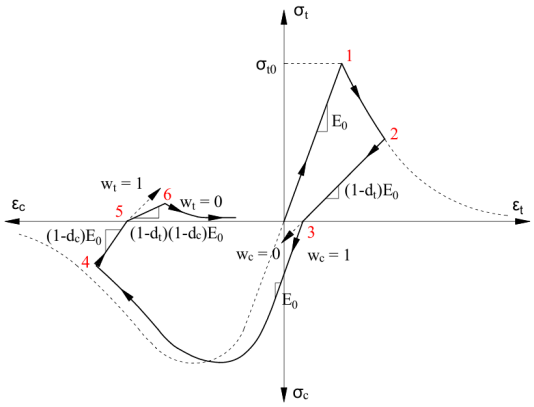

Figure 11. Concrete Uniaxial Cyclic Loading with Stiffness Recovery Factor Values [16]

Therefore, the value of tension stiffness recovery (w_t) is taken as 0. In contrast, during the transition from tension back to compression, the concrete cracks tend to close, partially restoring the stiffness of the material. Given that concrete damage in beam-column joints is generally more severe than at mid-span, a stiffness recovery value of 50% is adopted after crack closure. In this context, the compression stiffness recovery (w_c) is set to 0.5.

Reinforcing Bar Modeling

The behavior of reinforcing steel was modeled using a combined hardening plasticity approach, capturing both isotropic and kinematic effects. Isotropic hardening is defined by parameters $Q\infty$ and b, representing the maximum yield stress change and its rate of evolution, respectively. Kinematic hardening is characterized by C and γ, which govern the back stress modulus and saturation rate. The number of back stress components, N, was also specified. These parameters were adopted from previous research [10] based on their similarity to the material properties used in this research. They were evaluated through preliminary validation and found to provide acceptable agreement in the first stage model validation. The adopted values are summarized in Table 2.

Table 2. Combined Hardening Parameters

Reinforcement Type	f_y	N	C_k	γ_k	Q_∞	b
	MPa	-	MPa	-	MPa	-
Deformed	400	1	122400	430	35	1.12
Plain	240	5	456250	21538	225	12
			70520	3373		
			17380	1451		
			7670	771		
			5860	459		

Steel Deck Modeling

The steel deck is modeled using the constitutive steel model by Park and Paulay [11], with a yield strength of 250 MPa and ultimate strength of 287.5 MPa, as shown in Figure 12. While the profiling process may introduce strain ageing effects, such as increased yield strength and reduced ductility, these effects were not explicitly included. The steel deck was modeled using a general elastic–plastic representation, as adopted in the Park and Paulay model, which is considered adequate for capturing the global structural response in composite slab action. A similar simplified modeling approach was adopted in [17], where the steel deck was represented using a simplified elastic–plastic model.

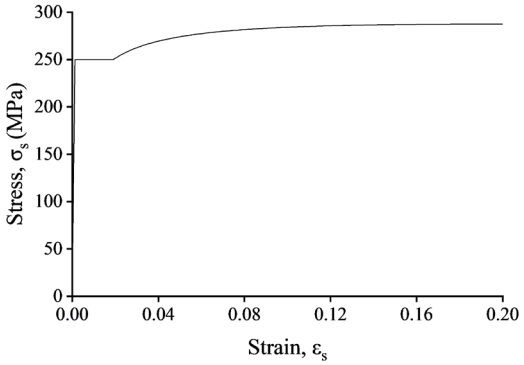

Figure 12. Steel Deck Material Model

Discrete Crack Modeling

The Concrete Damaged Plasticity (CDP) model often struggles to capture crack opening and closing under cyclic loading, as it relies on plastic strain accumulation rather than explicit crack modeling. This limitation leads to deviations in the compression response and overly rounded hysteresis curves, which can overestimate energy dissipation [18,19].

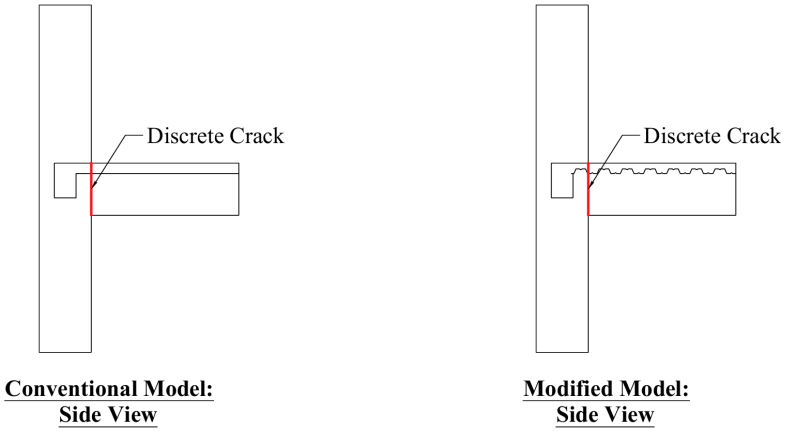

Figure 13. Discrete Crack Location

To overcome this, the discrete crack method was introduced by Chen [20] and later refined by Goto et al. [21,22], allowing explicit simulation of macro-cracks where tensile stress exceeds the concrete's tensile strength. Previous studies recommend introducing at least one discrete crack to accurately simulate hysteresis behavior under cyclic bending [21,22]. In this study, a single discrete crack is modeled using the penalty contact method with a hard normal contact interaction [23]. Its location is determined iteratively: an initial analysis without discrete cracks identifies regions of high tensile damage, followed by the placement of a crack at the beam-column interface, as illustrated in Figure 13.

Loading Scheme

The loading protocol follows FEMA 461, employing displacement control suitable for structural and non-structural element testing. This standard uses gradually increasing load amplitudes, with each level comprising two cycles and a minimum of 10 amplitude steps. The applied loading history is illustrated in Figure 14.

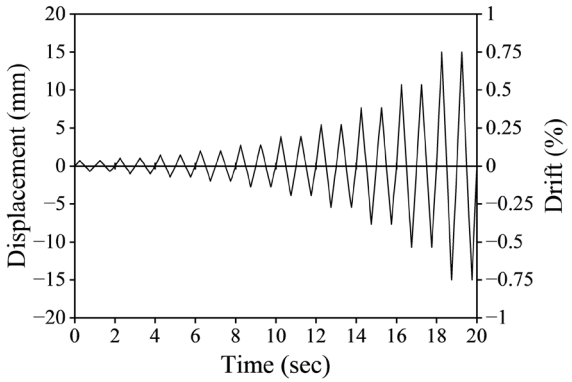

Figure 14. Cyclic Loading Protocol

RESULTS AND DISCUSSION

Comparison of the Conventional and Steel Deck Hysteresis Loops

The comparison of hysteresis loops between the conventional and modified models, as displayed in Figure 15, shows generally similar trends. Under positive loading, the modified model exhibits a slightly wider loop, reflecting greater energy dissipation and a higher damage level. In contrast, during negative loading, it shows reduced force response due to decreased effective concrete volume caused by the steel deck's profiled geometry, which accelerates damage propagation. The nominal strengths in the positive and negative directions for each model are denoted as P_n^+ and P_n^-, respectively. Overall, the modified model demonstrates slightly enhanced energy dissipation and ductility. However, more pronounced pinching effects at certain stages indicate greater stiffness degradation, influenced by bond-slip mechanisms and altered stress distribution at the concrete–steel deck interface.

The ultimate state evaluation under cyclic loading showed a maximum drift ratio of only 0.75%. At this stage, the longitudinal reinforcement had already attained its ultimate tensile strength (f_u), indicating that the existing structure does not yet satisfy the drift capacity requirements outlined in current design codes. Although the numerical model remained stable beyond this point, it is important to note that, in practice, reinforcement may experience necking or fracture once ultimate tensile strength is reached, potentially compromising structural integrity.

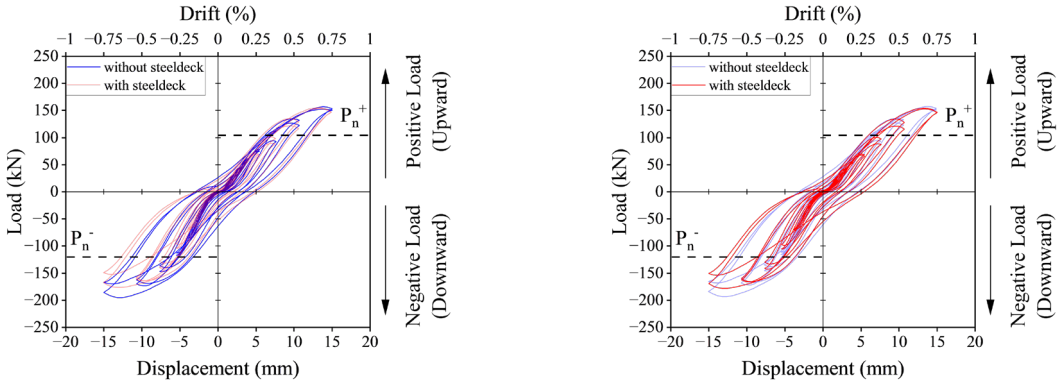

(a) Hysteresis Loop of Conventional Model (b) Hysteresis Loop of Modified Model

Figure 15. Hysteresis Loops

Initial Plastic Hinge Formation and First Yielding

Figure 16 and Figure **17** show the yield penetration lengths in the main beam for the conventional and modified models, respectively, highlighting the influence of slab configuration on yielding extent. The yield penetration was evaluated based on the distribution of plastic strain along the longitudinal reinforcement. For the bottom reinforcement, the yield length was assessed at the cycle just before reaching its ultimate tensile stress, while for the top reinforcement, it was observed at the peak negative amplitude prior to bottom bar failure.

The reinforcement yielding cycles for both top and bottom reinforcement are summarized in Table 3. In the modified model, all bottom reinforcing bars yielded at cycle 15, one cycle earlier than in the conventional model. Meanwhile,

the top reinforcement yielded almost simultaneously in both models. The earlier yielding of bottom reinforcement in the modified model indicates faster plasticization, attributed to geometric changes from the steel deck profile. The reduced concrete volume leads to a smaller compression block and an upward shift of the neutral axis, increasing tensile strain in the reinforcement and prompting earlier yielding.

Table 3. Reinforcement Yielding Cycles

Criteria	Cycle	
	Conventional Model	**Modified Model**
First bottom rebars yielding point	16	15
Total bottom rebars yielding	17	16
First top rebars yielding point	17	17

Table 4. Reinforcement Yield Penetration Lengths

Criteria	Yield Penetration Length	
	Conventional Model	**Modified Model**
	mm	*mm*
Average length of top rebars	119.42	299.33
Average length of bottom rebars	671.97	725.03

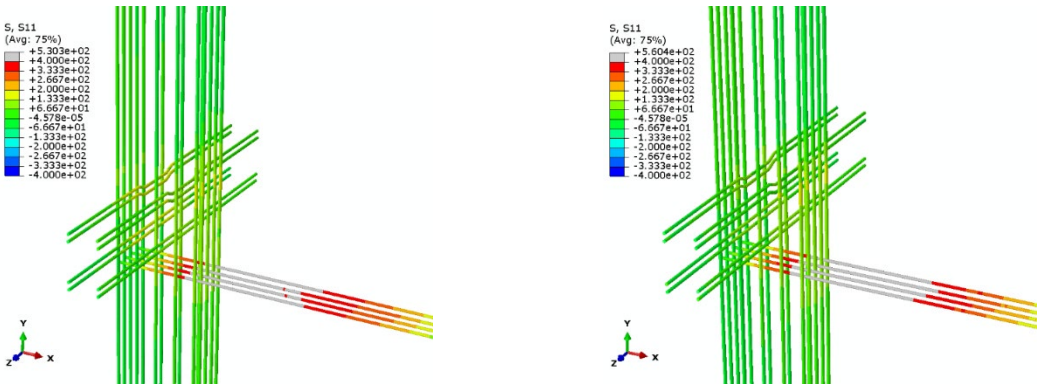

(a) Bottom Rebars of Conventional Model (b) Bottom Rebars of Modified Model

Figure 16. Yield Penetration Lengths of Bottom Rebars

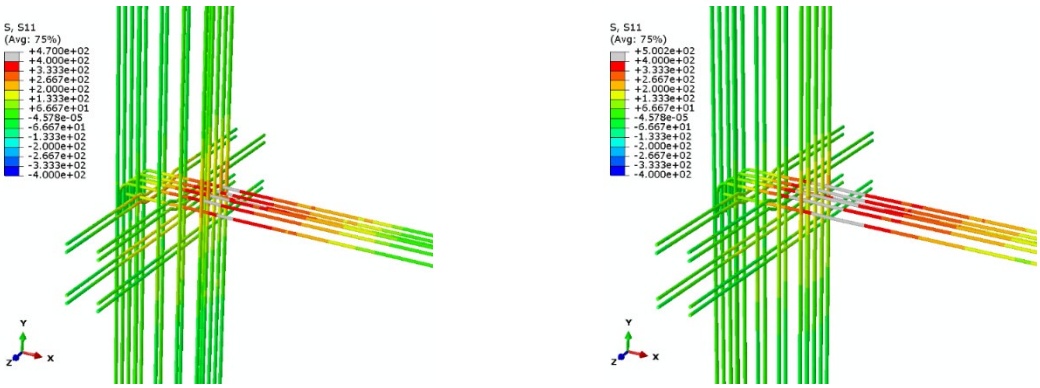

(a) Top Rebars of Conventional Model (b) Top Rebars of Modified Model

Figure 17. Yield Penetration Lengths of Top Rebars

As presented in Table 4, the modified model exhibits a longer yield penetration length in the bottom reinforcement, suggesting a more distributed plastic hinge zone. This behavior is attributed to the presence of the composite slab, which influences the flexural stiffness and moment distribution in the beam.

Energy Dissipation

Energy dissipation refers to energy lost or absorbed due to internal damage during loading, typically measured as the area under the hysteresis loop in cyclic loading, with the energy accumulated from each cycle to obtain the cumulative energy dissipation [24]. As shown in Figure 18, the modified model exhibits slightly higher cumulative energy dissipation (7293.62 J) than the conventional model (7120.92 J), indicating a greater capacity to absorb energy during

cyclic loading, with a 2.425% increase in energy dissipation. The greater energy dissipation in the modified model corresponds to its wider hysteresis loop, reflecting earlier inelastic deformation from premature reinforcement yielding and more pronounced pinching. This indicates an earlier transition to inelastic behavior and faster stiffness degradation compared to the conventional model.

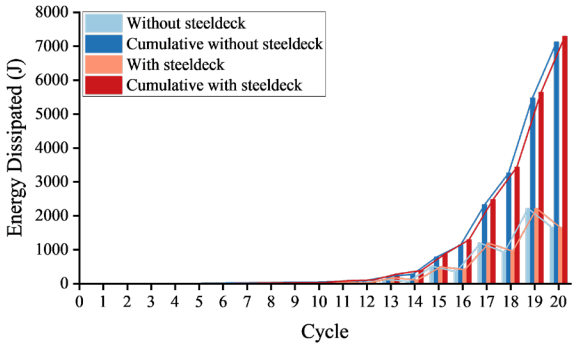

Figure 18. Energy Dissipation

Figure 18 shows low energy dissipation during the initial 10 cycles due to elastic behavior. A sharp increase follows, marking damage accumulation. The alternating rise and fall every two cycles align with the FEMA 461 protocol. Reduced hysteresis in second cycles indicates stiffness degradation from microcracking, reinforcement fatigue, and bond-slip, highlighting progressive damage under cyclic loading.

Ductility and Stiffness

Since ultimate strength (f_u) was reached during the final loading phase, displacement ductility was calculated using the final displacement as ultimate displacement. Yield displacement (δ_y) was obtained from the skeleton curve by fitting a tangent line to its linear segment, as shown in Figure 19 and Figure **20**, with the deviation point marking the yield point for determining both yield displacement (δ_y) and the corresponding load (F_y).

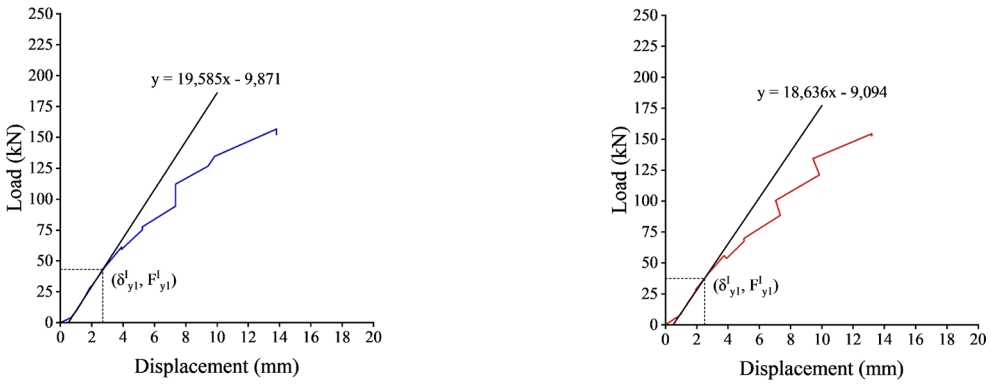

(a) Skeleton Curve of Conventional Model (b) Skeleton Curve of Modified Model

Figure 19. Skeleton Curve of Beam-Column Model in Positive Loading

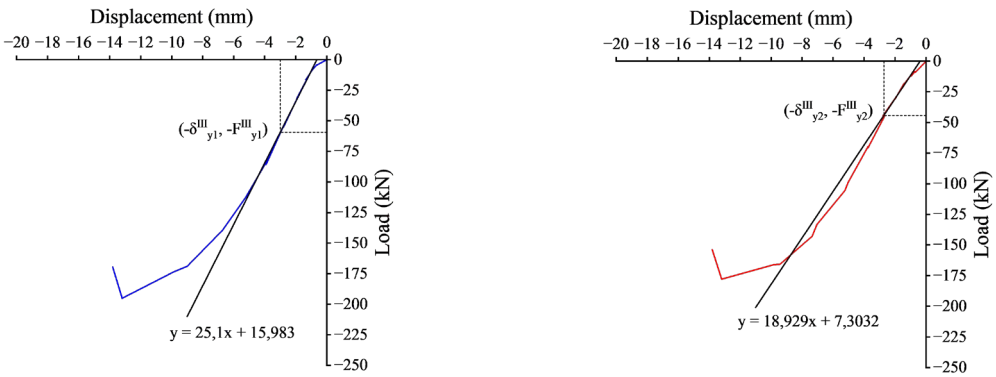

(a) Skeleton Curve of Conventional Model (b) Skeleton Curve of Modified Model

Figure 20. Skeleton Curve of Beam-Column Model in Negative Loading

Table 5. Ductility and Stiffness

Parameters	Loading Directions		Conventional Model	Modified Model	Difference
Displacement ductility ratio	Positive	-	5.1112	5.2800	3.303%
	Negative	-	4.4001	4.8353	9.890%
Elastic stiffness	Positive	kN/mm	15.9291	14.9984	-5.843%
	Negative	kN/mm	19.7723	16.2538	-17.795%
Inelastic stiffness	Positive	kN/mm	10.2477	10.9264	6.623%
	Negative	kN/mm	13.3256	12.7503	-4.317%

Table 5 presents the displacement ductility and stiffness ratios for both models. The modified model exhibits higher ductility, reflecting greater deformation capacity and energy dissipation, due to the ductile steel deck and reduced brittle concrete volume. It also shows lower initial elastic stiffness and faster degradation, mainly from increased concrete damage and bond-slip effects at the concrete–steel deck interface. Notably, in the positive direction, its inelastic stiffness is higher, suggesting better post-yield stiffness retention. While the conventional model shows a sharper stiffness drop, the modified model offers a more gradual transition, indicating improved post-yield behavior despite earlier stiffness loss. This highlights the steel deck system's enhanced ductility and energy absorption, albeit with earlier plastic deformation onset.

CONCLUSIONS

1. The modified model shows a slightly wider hysteresis loop with 2.425% higher cumulative energy dissipation than the conventional model. However, it exhibits sharper pinching and earlier stiffness degradation. Under negative loading, the modified model has a lower force response, indicating reduced tensile load-carrying capacity.
2. The modified model exhibits greater flexibility, with 3.303% and 9.89% higher positive and negative ductility ratios, respectively, but shows faster stiffness reduction from early loading. Conversely, the conventional model is stiffer in the elastic phase, by 5.843% and 17.795%, but suffers a more severe degradation after yielding. While the steel deck improves ductility and energy dissipation, it trades off with faster stiffness loss and lower elastic-phase strength.
3. The modified model exhibits earlier yielding in the bottom reinforcement, with all bars reaching yield sooner than in the conventional model. Top reinforcement yields after the bottom bars almost at the same time, indicating similar plastic hinge formation timing. However, the modified model enters the plastic phase earlier in tension.
4. Overall, the numerical analysis shows that using a steel deck as a composite slab has minimal impact on the plastic behavior at RC beam supports, with only slight differences in energy dissipation, ductility, stiffness, and plastic hinge formation time.

REFERENCES

1. Alva, G.M.S., El Debs, A.L.H. de C., and El Debs, M.K., An Experimental Study on Cyclic Behaviour of Reinforced Concrete Connections, *Canadian Journal of Civil Engineering*, 34, 2007, pp. 565–575, doi: https://doi.org/10.1139/L06-164.
2. Diro, G.A. and Kabeta, W.F., Finite Element Analysis of Key Influence Parameters in Reinforced Concrete Exterior Beam Column Connection subjected to Lateral Loading, *European Journal of Engineering and Technology Research*, 5(6), 2020, pp. 689–697, http://dx.doi.org/10.24018/ejeng.2020.5.6.1947.
3. Sabah, H.A.H. and Harba, I.S.I., Numerical Analysis of Reinforced Concrete Exterior Beam-Column Joints under Limited Cycles of Repeated Loading, *Diyala Journal of Engineering Sciences*, 15(4), 2022, pp. 108–129, https://doi.org/10.24237/djes.2022.15410.
4. Durrani, A.J. and Zerbe, H.E., Seismic Resistance of R/C Exterior Connections with Floor Slab, *Journal of Structural Engineering*, 113*(*8), 1987, pp. 1850–1864, https://doi.org/10.1061/(ASCE)0733-9445(1987)113:8(1850).
5. Kalogeropoulos, G., Tsonos, A.D., and Iakovidis, P., Hysteresis Behavior of RC Beam–Column Joints of Existing Substandard RC Structures Subjected to Seismic Loading–Experimental and Analytical Investigation, *Buildings*, 14(6), 2024, pp. 1609, https://doi.org/10.3390/buildings14061609.
6. Eissa, M. and Celikag, M., Composite Behavior of Reinforced Concrete T-Beam with Composite Slab, *Arabian Journal for Science and Engineering*, 47(10), 2022, pp. 13073–13093, https://doi.org/10.1007/s13369-022-06699-4.
7. Sidara, S.C.X., Sumajouw, M.D.J., and Pandaleke, R., Evaluasi Kekuatan Balok Beton Bertulang dengan Balok

Komposit Baja Menggunakan Floor Deck, *Jurnal Sipil Statik*, 5(9), 2017, pp. 579–590.
8. Hedaoo, N.A., Gupta, L.M., and Ronghe, G.N., Design of Composite Slabs with Profiled Steel Decking: A Comparison between Experimental and Analytical Studies, *International Journal of Advanced Structural Engineering*, 3(1), 2012.
9. Mander, J.B., Priestley, M.J.N., and Park, R., Theoretical Stress-Strain Model for Confined Concrete, *Journal of Structural Engineering*, 114(8), 1988, pp. 1804–1826, https://doi.org/10.1061/(ASCE)0733-9445(1988)114:8(1804).
10. Narendra, P.V.R., Prasad, K., Krishna, E.H., Kumar, V., and Singh, K.D., Low-Cycle-Fatigue (LCF) Behavior and Cyclic Plasticity Modeling of E250A Mild Steel, *Structures*, 20, 2019, pp. 594–606, https://doi.org/10.1016/j.istruc.2019.06.014.
11. Park, R. and Paulay, T., *Reinforced Concrete Structures*, John Wiley & Sons, Inc., Canada, 1975.
12. Majdi, Y., Hsu, C.T.T., and Punurai, S., Local Bond-slip Behavior between Cold-formed Metal and Concrete, *Engineering Structures*, 69, 2014, pp. 271–284, https://doi.org/10.1016/j.engstruct.2014.03.025.
13. Gosztola, D., Cucuzza, R., Szép, J., Domaneschi, M., Ghodousian, O., and Movahedi Rad, M., Plastic Limited Numerical Modelling on Contact Friction Effects of Steel–Concrete Connection for Composite Bridges, *Buildings*, 14(9), 2024, doi: https://doi.org/10.3390/buildings14092898.
14. Alfarah, B., López-Almansa, F., and Oller, S., New Methodology for Calculating Damage Variables Evolution in Plastic Damage Model for RC Structures, *Engineering Structures*, 132, 2017, pp. 70–86, https://doi.org/10.1016/j.engstruct.2016.11.022.
15. Alfarah, B., Murcia-Delso, J., López-Almansa, F., and Oller, S., RC Structures Cyclic Behavior Simulation with a Model Integrating Plasticity, Damage, and Bond-Slip, *Earthquake Engineering & Structural Dynamics*, 47(2), 2017, pp. 1–19, https://doi.org/10.1002/eqe.2974.
16. Dassault Systèmes, *SIMULIA User Assistance 2020*, Dassault Systèmes, 2020.
17. Abdullah, R., Paton-Cole, V.P., and Easterling, W.S., Quasi-static Analysis of Composite Slab, *Malaysian Journal of Civil Engineering*, 19(2), 2007, pp. 91–103.
18. Yu-Hang, W., Qi, T., and Xin, N., Comparative Investigation on Influences of Concrete Material Constitutive Models on Structural Behavior, *Construction and Building Materials*, 144, 2017, pp. 475–483, http://dx.doi.org/10.1016/j.conbuildmat.2017.03.174.
19. Wang, J.J., Liu, C., Fan, J.S., Hajjar, J.F., and Nie, X., Triaxial Concrete Constitutive Model for Simulation of Composite Plate Shear Wall–Concrete Encased: THUC3, *Journal of Structural Engineering*, 145(9), 2019, https://doi.org/10.1061/(ASCE)ST.1943-541X.0002355.
20. Chen, W.F., *Plasticity in Reinforced Concrete*, McGraw-Hill, New York, 1982.
21. Goto, Y., Mizuno, K., and Prosenjit Kumar, G., Nonlinear Finite Element Analysis for Cyclic Behavior of Thin-Walled Stiffened Rectangular Steel Columns with In-Filled Concrete, *Journal of Structural Engineering*, 138, 2012 pp. 571–584, https://doi.org/10.1061/(ASCE)ST.1943-541X.0000504.
22. Goto, Y., Kumar, G.P., and Kawanishi, N., Nonlinear Finite-Element Analysis for Hysteretic Behavior of Thin-Walled Circular Steel Columns with In-Filled Concrete, *Journal of Structural Engineering*, 136, 2010, pp. 1413–1422, https://doi.org/10.1061/(ASCE)ST.1943-541X.0000240.
23. Hou, H., Wang, W., and Wang, S., Nonlinear Modeling Methods for Cyclic Analysis of Double-Skin Composite Shear Walls, *Thin-Walled Structures*, 187, 2023, https://doi.org/10.1016/j.tws.2023.110737.
24. Rodrigues, H., Varum, H., Arêde, A., and Costa, A., A Comparative Analysis of Energy Dissipation and Equivalent Viscous Damping of RC Columns subjected to Uniaxial and Biaxial Loading, *Engineering Structures*, 35, 2012, pp. 149–164, https://doi.org/10.1016/j.engstruct.2011.11.014.